Loss of TIGAR Induces Oxidative Stress and Meiotic Defects in Oocytes from Obese Mice*[S]

Haichao Wang‡‡‡, Qing Cheng§‡‡, Xiaoyan Li‡¶, Feifei Hu‖, Longsen Han‡, Hao Zhang‡, Ling Li‡, Juan Ge‡, Xiaoyan Ying‖, Xuejiang Guo‡**, and Qiang Wang‡**

Maternal obesity has been reported to impair oocyte quality in mice, however, the underlying mechanisms remain unclear. In the present study, by conducting a comparative proteomic analysis, we identified a reduced expression of TIGAR (TP53-induced glycolysis and apoptosis regulator) protein in ovulated oocytes from high-fat diet (HFD)-fed mice. Specific depletion of TIGAR in mouse oocytes results in the marked elevation of reactive oxygen species (ROS) levels and the failure of meiotic apparatus assembly. Importantly, forced expression of TIGAR in HFD oocytes not only attenuates ROS production, but also partly prevents spindle disorganization and chromosome misalignment during meiosis. Meantime, we noted that TIGAR knockdown in oocytes induces a strong activation of autophagy, whereas overexpression of TIGAR significantly reduces the LC3 accumulation in HFD oocytes. By anti-oxidant treatment, we further demonstrated that such an autophagic response is dependent on the TIGAR-controlled ROS production. In summary, our data indicate a role for TIGAR in modulating redox homeostasis during oocyte maturation, and uncover that loss of TIGAR is a critical pathway mediating the effects of maternal obesity on oocyte quality. ***Molecular & Cellular Proteomics 17: 1354–1364, 2018. DOI: 10.1074/mcp.RA118.000620.***

As the prevalence of obesity is increasing in all populations, the proportion of reproductive age women who are becoming overweight and obese is rising (1, 2). Substantial studies have demonstrated that excessive body fat has a detrimental effect on female fertility and pregnancy (3). For example, obesity is associated with increased risks of infertility, miscarriage, congenital abnormalities in the offspring, and impaired pregnancy success using assisted reproductive technologies (ART)[1] (2, 4–8). Emerging evidence derived from oocyte donation and embryo transfer experiments indicate poor oocyte quality accounts, at least in part, for those defective phenotypes in obese females (6, 10). We and others have reported that maternal obesity impairs the developmental competence of oocytes, resulting in meiotic anomalies, mitochondrial dysfunction, as well as oxidative stress (3, 6, 11). The major sources of reactive oxygen species (ROS) production are mitochondrial oxidative respiration (12, 13), where they are generated because of release of electrons from the electron transport chain (12, 14). However, excessive amounts of ROS can be damaging to the cell, inducing DNA damage, lipid oxidation, and, ultimately, cell death (15). Despite numerous studies suggest that oxidative stress may be a link between maternal obesity and oocyte quality, the potential factors mediating this process remain to be explored.

TIGAR (TP53-induced glycolysis and apoptosis regulator) was initially found to be a product of a p53 target gene, which shares functional sequence similarities with the bisphosphatase domain of the bifunctional enzyme PFK-2/FBPase-2 (6-phosphofructo-2-kinase/fructose-2,6-bisphosphatase) (16–18). TIGAR has been demonstrated to act as a negative regulator of glycolysis by lowering intracellular levels of fructose-2,6-bisphosphate, leading to the pentose phosphate pathway (PPP) activation and NADPH production (16). TIGAR was also found to protect glioma cells from hypoxia- and ROS-induced cell death by stimulating mitochondrial energy metabolism and oxygen consumption in a p53/TP53-independent manner (19). A recent report showed that TIGAR has a dual role in cancer cell survival through inhibiting both apoptosis and autophagy in response to tumor chemotherapy (20). It is interesting to note that PPP plays an important role in controlling nuclear and cytoplasmic maturation of mammalian oocytes (21–23). Inhibition of PPP modifies the pattern of oxidation and mitochondrial fluctuation, resulting in impaired meiotic progression in oocytes (24). Moreover, activity of glucose 6-phosphate dehydrogenase (G6PDH), the rate-limiting enzyme in PPP, has been widely used to evaluate the developmental competence of oocytes from different species (25). However, to date, whether TIGAR functions during mammalian oocyte development, and if so how it determines oocyte

From the ‡State Key Laboratory of Reproductive Medicine, Nanjing Medical University; §Departement of Obstetrics, Obstetrics and Gynecology Hospital Affiliated to Nanjing Medical University; ¶College of Animal Science & Technology, Nanjing Agricultural University; ‖Department of Obstetrics and Gynecology, The Second Affiliated Hospital of Nanjing Medical University, Nanjing, China, 210000

Received January 16, 2018, and in revised form, April 25, 2018
Published, MCP Papers in Press, May 18, 2018, DOI 10.1074/mcp.RA118.000620

competence and even offspring phenotype, are completely unknown.

In the present study, by performing a comparative proteomic analysis, we identified a significant reduction of TIGAR protein in matured oocytes from obese mice. We further investigated the role of TIGAR during mouse oocyte maturation employing *in vitro* knockdown and overexpression assays. Notably, forced expression of TIGAR could protect oocytes from obese mice against oxidative stress and meiotic defects.

EXPERIMENTAL PROCEDURES

All chemicals and culture media were purchased from Sigma (St. Louis, MO) unless stated otherwise.

Animals and Diet—All experiments were approved by the Animal Care and Use Committee of Nanjing Medical University and were performed in accordance with institutional guidelines. Female ICR mice age 3 weeks were housed 5 per cage and given access to water and fed either a high-fat diet (HFD) containing 35.8% fat, 20.7% protein, and 35% carbohydrates (D12492; Research Diets, New Brunswick, NJ), or a control diet (Control) containing 4.8% fat, 73.9% carbohydrate, and 14.8% protein *ad libitum*. After 16 weeks of feeding, body weights (33.6 $\pm$ 1.3 g, $n = 10$ control *versus* 54.3 $\pm$ 3.3 g, $n = 10$ HFD; $p < 0.05$) and fasting serum glucose (92 $\pm$ 6.9 mg/dL, $n = 10$ control *versus* 140.7 $\pm$ 2.8 mg/dL, $n = 10$ HFD; $p < 0.05$) were significantly higher in mice fed a HFD compared with controls.

Antibodies—Rabbit polyclonal anti-TIGAR antibody (Cat#: ab62533) was purchased from Abcam (Cambridge, MA); Mouse monoclonal anti-α-tubulin-FITC antibody (Cat#: F2168) was purchased from Sigma; Rabbit monoclonal anti-microtubule-associated protein 1 light chain 3 (LC 3) antibody (Cat#: 3868S) was purchased from Cell Signaling Technology (Danvers, MA). FITC-conjugated goat anti-rabbit IgG was purchased from Thermo Fisher Scientific (Cat# 65–6111; Rockford, IL).

Oocyte Collection and Culture—Female mice were superovulated with 5 IU Pregnant Mares Serum Gonadotropin (PMSG) by intraperitoneal injection, and 48 h later, cumulus-oocyte complexes were collected by manual rupturing of antral follicles. With gentle washes by pipetting, cumulus cells were removed and denuded GV oocytes were obtained. For *in vitro* maturation, fully-grown GV oocytes were cultured in M16 medium under mineral oil at 37 °C in a 5% CO_2 incubator. To collect ovulated MII oocytes, mice received an injection of 5 IU human Chorionic Gonadotropin (hCG) after PMSG priming. Oocytes were retrieved from oviduct ampullae 13.5 h post-hCG, and freed of cumulus cells by exposure to 1 mg/ml hyaluronidase.

LC-MS/MS Analysis—Samples were lysed and trypsin digested according to our previous procedure (26, 27). Briefly, purified peptides were loaded onto a trap column (75 μm$\times$2 cm, Acclaim® PepMap100 C18 column, 3 μm, 100 Å; DIONEX, Sunnyvale, CA), and then separated with a reverse-phase analytical column (75 μm$\times$25 cm, Acclaim® PepMap RSLC C18 column, 2 μm, 100 Å; DIONEX) using a Proxeon Easy-nLC 1000 system. The effluent from LC column was coupled directly to a LTQ OrbitrapVelos mass spectrometer (Thermo Finnigan, San Jose, CA). The reverse-phase separation of peptides was performed using the following mobile phase components: 0.1% FA (buffer A) and 100% ACN, 0.1% FA (buffer B). The gradient elution conditions (240 min total) were: 3% to 5% buffer B for 5 min; 5% to 30% buffer B for 205min ; 30% to 45% buffer B for 21 min; 45% to 90% buffer B for 1 min; and 90% buffer B for 8min. The parameter settings for mass spectrometer were referred to our published reports (26, 27).

Protein Identification and Quantification—Raw files were processed using MaxQuant (Version 1.2.2.5) (28), and searched against the mouse protein sequence database from UniProt (release 2013_12; 87187 sequences) (29), combined with the standard contaminants database embedded in MaxQuant. The false discovery rate (FDR) of the identification was estimated by searching against the databases with the reversed protein sequences. The FDR values for peptide and protein were both set to 0.01. Enzyme specificity was full cleavage by trypsin, with two maximum missed cleavage sites. The minimum peptide length required was six amino acids. Carbamidomethyl (C) was set as a fixed modification. Variable modifications included Oxidation (M) and Acetyl (Protein N-term). The mass tolerance for precursor ions was set to 20 ppm at the first search as applied in Maxquant for initial mass recalibration. For the main search, the mass tolerance for precursor ions was set to 6 ppm. The mass tolerance for fragment ions was set to 0.5 Da. For label free quantification, protein expression levels were estimated using the iBAQ (Intensity Based Absolute Quantification) algorithm embedded in MaxQuant (30). In brief, protein expression level was calculated by the sum of peak intensities (normalized by the number of theoretically observable peptides) of all peptides matching to the corresponding protein. The value of iBAQ is proportional to the relative expression level of protein. We further normalized the expression levels of each sample by dividing each raw iBAQ value by the median value.

Bioinformatic Analysis—A volcano plot was constructed to better visualize and identify the differentially expressed proteins between groups. Hierarchical clustering analysis was carried out using Cluster3.0 software (31), and a heat map was produced accompanied by a dendrogram depicting the extent of similarity of protein expression among the samples. For the convenience of gene annotation, corresponding Ensembl gene IDs of the differentially expressed proteins were used for further bioinformatics analysis. To characterize these genes, we tested them for enrichment of gene ontology (GO) biological process, cellular component, and molecular function terms by using DAVIDs Functional Annotation Chart tool (Version 6.8)(32). A p value less than 0.05 was controlled for significant enrichment. An important portion of enriched GO terms were selected to construct a network with related proteins using Cytoscape.

Experimental Design and Statistical Rationale—Emerging evidence supports that maternal obesity exerts its effects on embryo development through the factors within the oocyte. To identify such potential effectors, the high-throughput proteomics analysis was performed on ovulated MII oocytes collected from HFD and control mice (300 oocytes from 15 mice for each sample). A total of four HFD biological replicates and five control biological replicates were used. The unpaired Student's t test was used to compare mean values of each protein between groups. For the identification of differentially expressed proteins, the cutoffs for the fold change and p value were set to 1.5 and 0.05, respectively. For the cell biology assays, all experiments were repeated three times and data were expressed as mean $\pm$ S.D. $p < 0.05$ was significant.

Plasmid Construction and mRNA Synthesis—Total RNA was extracted from 100 denuded oocytes using an Arcturus PicoPure RNA isolation kit (Applied Biosystems, Foster City, CA), and the cDNA was generated with QuantiTect Reverse Transcription kit (Qiagen, Hilden, Germany). The following primers were used to amplify the CDS sequence of TIGAR: forward primer, 5′-GGGGGCCGGCCCAGGCAAAGTGGTCCCAGAG-3′, and reverse primer, 5′-GGGGGCGCGCCAGCAGCAGAGGCCAAGTCC-3′. PCR products were purified, di-

[1] The abbreviations used are: ART, assisted reproductive technology; GV, germinal vesicle; MI, metaphase I; MII, metaphase II; Pb1, first polar body; PMSG, pregnant mare serum gonadotropin; hCG, human chorionic gonadotropin; LH, luteinising hormone; PI, propidium iodide; ROS, reactive oxygen species; HFD, high-fat diet; NAC, N-acetyl-L-cystein.

gested with *Fse*I and *Asc*I (New England Biolabs, Ipswich, MA), and then cloned into the pCS2$^+$ vector. For the synthesis of TIGAR mRNA, the TIGAR-pCS2$^+$ plasmids were linearized by SacII. Capped cRNAs were produced using *in vitro* transcription with SP6 mMESSAGE mMACHINE (Ambion, Carlsbad, CA) according to the manufacturer's instructions. Synthesized RNA was aliquoted and stored at −80 °C.

Knockdown and Overexpression Analysis—Microinjections of siRNA or mRNA, with a Narishige (Tokyo, Japan) microinjector, were used to knock down or overexpress TIGAR in mouse oocytes, respectively. For overexpression experiments, 10 pl TIGAR mRNA solution (10 ng/μl) was injected into cytoplasm of GV oocytes. The same amount of RNase-free PBS was injected as control. For knockdown experiments, TIGAR-targeting siRNA was diluted with water to give a stock concentration of 1 mM, and 2.5 pl solution was injected. The siRNA pairs used were as follows: 5′-GCGAUCUCACGAGGACUAATT-3′ (forward strand) and 5′-UUAGUCCUCGUGAGAUCGCTT-3′ (reverse strand). A nonspecific siRNA as a negative control was also used in the present study (forward strand: 5′-UUCUCCGAACGUGUCACGUTT-3′; reverse strand: 5′-ACGUGACACGUUCGGAGAATT-3′).

The injected oocytes were arrested at GV stage in medium containing 2.5 μM milrinone, a phosphodiesterase inhibitor that blocks meiotic maturation, for 20 h, to allow time for siRNA-mediated knockdown or to permit overexpression. Then oocytes were washed three times in medium without milrinone, and *in vitro* cultured for the experimental analysis.

Western Blotting—Pool of oocytes was lysed in Laemmli sample buffer with protease inhibitor, heated at 100 °C for 5 min and separated by sodium dodecyl sulfate- polyacrylamide gel electrophoresis (SDS-PAGE). The separated proteins were transferred to polyvinylidene fluoride (PVDF) membranes. After blocking in Tris-buffered saline and containing 0.1% Tween 20 (TBST) with 5% skim milk for 1 h, the membranes were incubated with TIGAR antibodies (1:1000) or LC3B antibodies (1:1000) at 4 °C overnight. Membranes were washed in TBST three times, 10 min each, followed by incubation with horseradish peroxidase (HRP)-conjugated secondary antibodies for 1 h at room temperature. Finally, the protein bands were visualized using an ECL Plus Western blotting Detection System. The membrane was then washed and reblotted with anti-β-actin (1:5000) antibody as a loading control. All Western blotting experiments were repeated at least three times.

Measurement of Intracellular ROS—Intracellular ROS levels were determined by CM-H_2DCFDA (Life Technologies, Invitrogen TM, Carlsbad, CA, Cat#: C6827). CM-H_2DCFDA was prepared in DMSO prior to loading. Oocytes were incubated in M16 medium containing 5 mM CM-H_2DCFDA for 30 min at 37 °C in a 5% CO_2 incubator. Following three washes in PBS, 5–10 oocytes were loaded on a slide with a microdrop of medium, and immediately observed under a Laser Scanning Confocal Microscope (LSM 710, Zeiss, Oberkochen, Germany). Assays were performed in triplicates.

Immunofluorescence—Oocytes were fixed in 4% paraformaldehyde for 30 min, permeabilized in 0.5% Triton-X 100 for 20 min at room temperature, then treated with blocking solution (1% BSA-supplemented PBS) for 1 h. Oocytes were subjected to indirect immunofluorescence staining by incubating overnight at 4 °C with primary antibodies as follows: anti-TIGAR antibody (1:50, Abcam), anti-LC3 antibody (1:200, CST), FITC-conjugated anti-tubulin antibody (1:200, Sigma). After washing three times, samples were incubated with an appropriate secondary antibody for 1 h at room temperature. Chromosomes were stained using propidium iodide (PI; red) or Hoechst 33342 (blue) for 10 min. Finally, oocytes were mounted on anti-fade medium (Vectashield, Burlingame, CA), and examined under a Laser Scanning Confocal Microscope (LSM 710) equipped with the 40× objectives. ImageJ software (U.S. National Institutes of Health, Bethesda, MD) was used to quantify the intensity of fluorescence as described previously (33).

RESULTS

Comparative Proteomic Analysis of Ovulated Oocytes from Control and Obese Mice—To establish an obese mouse model, female mice were continuously fed with a high-fat diet (HFD) or a normal diet (control) for 16 weeks beginning at 3 weeks of age. In this paper, these mice are termed "HFD mice" and "control mice," respectively. Accordingly, we call their oocytes "HFD oocytes" and "control oocytes." Substantial evidence indicates that the effects of maternal obesity on embryo/offspring development can be attributed to factors within the oocyte (6). High-throughput proteomics technologies combining with advanced bioinformatics are extensively used to identify essential proteins in cellular events and molecular signatures of diseases (34). Here, to identify such potential effectors, liquid chromatography-tandem mass spectrometry (LC-MS) analysis was performed on the ovulated MII oocytes from control and HFD mice.

A total of 1142 proteins were identified, and 1137 proteins were quantified in oocytes. Using a cut-off for the fold change $>$ 1.5 and significance p values of $<$ 0.05, 111 proteins were identified as differentially expressed (DE) between groups (supplemental Table S1) (35). Of them, 43 proteins were up-regulated and 68 proteins were downregulated in HFD oocytes compared with their controls (Fig. 1*A*–1*B*). To obtain an overview of the function of DE proteins, gene ontology (GO) enrichment analysis was conducted (supplemental Table S2). Subcellular distribution of DE proteins was annotated using GO with database for annotation, visualization, and integrated discovery (DAVID). As shown in Fig. 1*C*, the largest proportion of DE proteins identified was annotated as cytoplasm (89), followed by nucleus (51), vesicle (43), and mitochondrion (31). Major GO terms including the related annotated proteins were also presented as a network. DE proteins were found to be enriched in cytoskeletal regulation, mitochondria-mediated events, and oxidation-reduction process (Fig. 1*D*).

Of these DE proteins, TIGAR (-1.9 fold change, $p = 0.0079$) is of great interest because: (1) TIGAR is a mitochondrion protein essential for cellular ROS homeostasis; (2) TIGAR modulates PPP pathway, a critical metabolic pathway determining mammalian oocyte quality. Although TIGAR has been reported to function in the control of redox status in several cell types (15, 19), its role in mammalian oocytes remains unknown. Moreover, to date, few factor(s) were identified to induce the oxidative stress in HFD oocytes. Thus, we decided to first focus on the functional exploration of TIGAR in mouse oocytes.

Loss of TIGAR Protein in Oocytes from HFD Mice—To validate the results of proteomic analysis, we further examined the TIGAR expression difference by Western blot analysis, and found a ~60–70% reduction in HFD oocytes com-

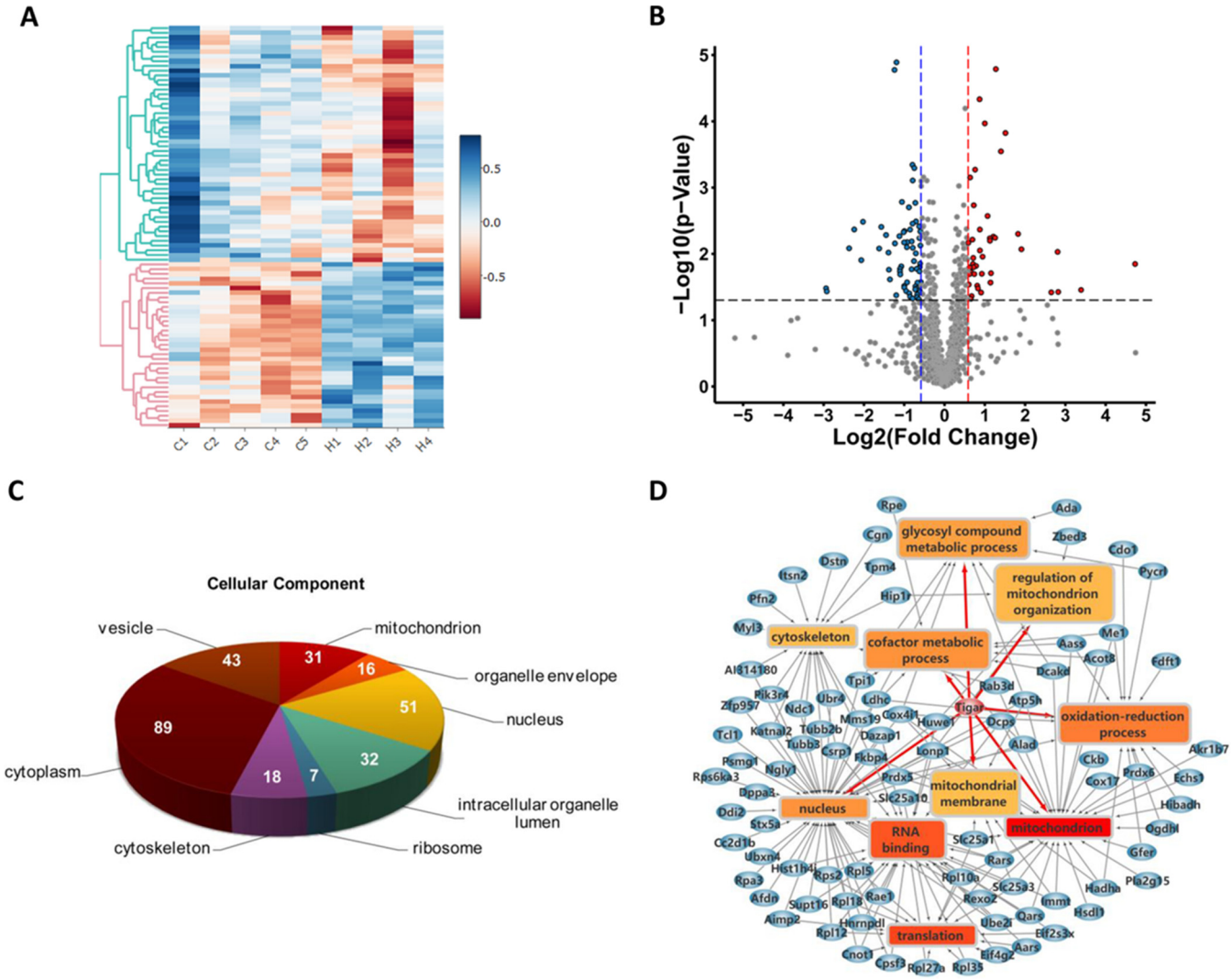

FIG. 1. **Proteomics analysis of ovulated oocytes from control and HFD mice.** *A*, Heatmap of the differentially expressed proteins between control and HFD groups. H1-H4: oocytes from HFD mice, C1-C5: oocytes from control mice. *B*, Volcano plot showing the quantitative protein expression in oocytes from control and HFD mice. Proteins differentially expressed with fold change over 1.5 were marked in color. *C*, Subcellular distribution of the differentially expressed proteins. *D*, Network of gene ontology and related differential proteins between control and HFD mice in oocytes.

pared with control oocytes (Fig. 2*A*–2*B*). Quantitative analysis based on staining also showed that the average fluorescence intensity of TIGAR in HFD oocytes was significantly decreased relative to controls (Fig. 2*C*–2*D*), in line with the Western blotting data.

Accompanying with germinal vesicle breakdown (GVBD), fully-grown oocytes reinitiate meiosis. Microtubules organize into the meiosis I (MI) spindle, chromosomes align at the metaphase plate, and then oocytes proceed through MI division. Following the emission of first polar body (Pb1), oocytes are arrested at metaphase II (MII) awaiting fertilization. To explore the potential function of TIGAR during oocyte maturation, we then examined its subcellular distribution at distinct stages. Immunostaining clearly showed that TIGAR predominantly resides in the cytoplasm of GV oocytes. However, as the oocytes enter meiosis, TIGAR becomes concentrated on the spindle region from pre-metaphase I to metaphase II stages (Fig. 2E, arrowheads). Such a specific distribution pattern implies that TIGAR may be involved in regulation of meiotic maturation. On this basis, the loss of TIGAR protein is likely to be a contributory factor compromising oocyte quality in obese mice.

Depletion of TIGAR Adversely Affects Meiotic Progression—To investigate the functional involvement of TIGAR in oocyte meiosis, fully-grown oocytes were microinjected with *TIGAR*-targeting siRNA (TIGAR-siRNA). This led to a significant reduction of TIGAR protein based on Western blot analysis (Fig. 3*A*–3*B*). Next, we evaluated how TIGAR knockdown affects the maturational progression of mouse oocytes. After 3 h *in vitro*-culture, both control and TIGAR-

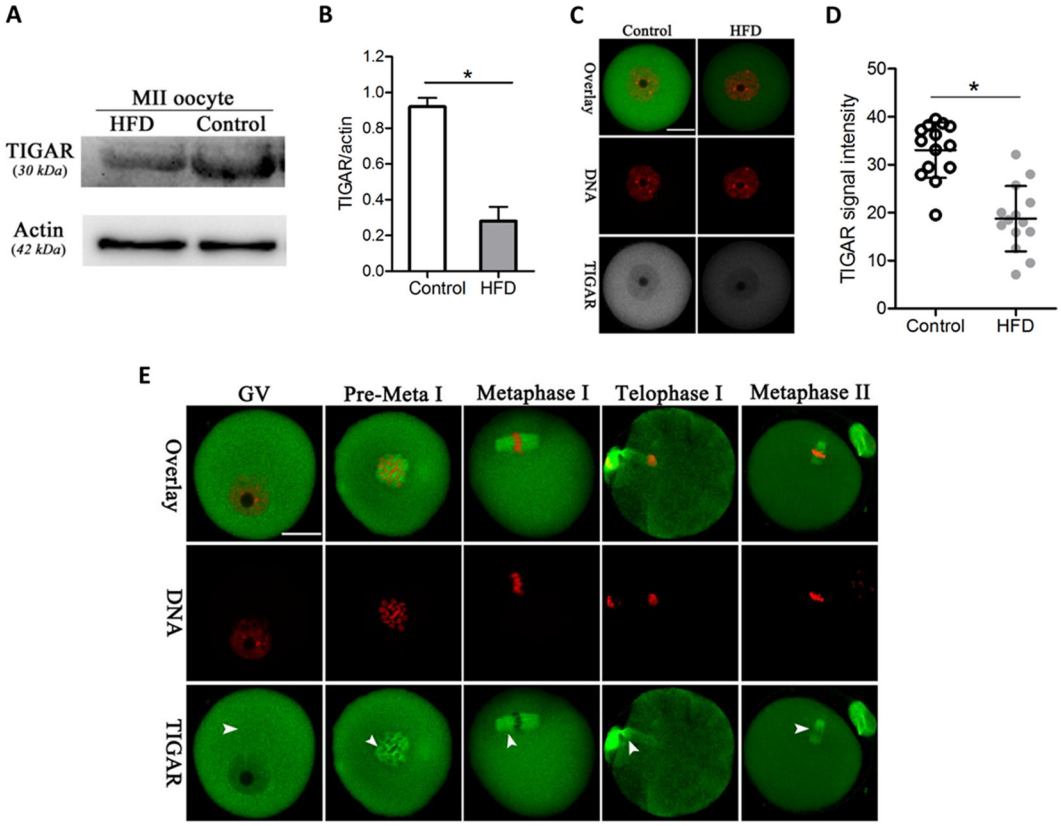

FIG. 2. **Reduced TIGAR expression in oocytes from HFD mice.** *A*, Western blot analysis confirmed the reduced TIGAR expression in oocytes from HFD mice compared with controls (100 oocytes for each group). *B*, The ratio of TIGAR/Actin intensity from Western blotting shown in *A*. Band intensity was calculated using ImageJ software, with actin as a loading control. *C*, Representative confocal sections of control and HFD oocytes labeled with anti-TIGAR antibody (green) and counterstained with propidium iodide (red) for DNA are shown. *D*, Quantification of TIGAR fluorescence shown in *C* ($n = 15$ for each group). *E*, Oocytes from control mice at GV, pre-metaphase I, metaphase I, telophase I, and metaphase II stages were immunolabeled with anti-TIGAR antibody (green) and counterstained with propidium iodide to visualize DNA (red). Arrowheads point to TIGAR signals. All experiments were repeated three times and representative images shown. Data were expressed as mean ± S.D. *$p < 0.05$. Scale bar: 20 μm.

siRNA oocytes resume meiosis normally, evidenced by the similar GVBD rate (80.7 ± 2.2% *versus* 89.2 ± 1.5% control, $p > 0.05$; Fig. 3*C*). However, after 14 h, the ratio of Pb1 extrusion was significantly decreased in TIGAR-depleted oocytes compared with controls (46.5 ± 3.1% *versus*84.1 ± 2.2% control, $p < 0.05$; Fig. 3*D*), with a high frequency of symmetric division (3.3 ± 0.5% *versus*19.6 ± 2.5% control, $p < 0.05$; Fig. 3*E*, pink asterisks). Together, these results suggest that TIGAR is essential for oocyte maturation and meiotic division.

TIGAR Modulates ROS Generation in Mouse Oocytes—Numerous studies have shown that TIGAR is associated with redox homeostasis in diverse cell types (15, 19, 36, 37). Hence, here we wished to determine whether TIGAR expression is required for ROS generation during mouse oocyte maturation. To do this, live oocytes were stained with CM-H_2DCFDA, a dye that fluoresces when oxidized by ROS, and then examined under confocal microscope. Consistent with our previous data (38), HFD oocytes showed significantly more ROS than controls, as determined by mean fluorescence (Fig. 4*A*a,c and 4*B*). Of note, we found that knockdown of TIGAR resulted in the increased ROS content in both control and HFD oocytes (Fig. 4*A*b,d and 4*B*). Moreover, to test whether elevating TIGAR expression can ameliorate oxidative stress in HFD oocytes, we carried out overexpression experiments by injecting exogenous TIGAR mRNA into oocytes. TIGAR overexpression had little effects on ROS content in normal oocytes likely because of the low basal level (Fig. 4*C*a,b-4*D*). By contrast, forced expression of TIGAR in HFD oocytes strikingly reduced the ROS levels after *in vitro* maturation (Fig. 4*C*c,d-4*D*), providing additional support that loss of TIGAR contributes to excessive ROS production in HFD oocytes. Taken together, these results demonstrate that TIGAR modulates redox homeostasis in mouse oocytes and protects oocytes against oxidative stress under obese environment.

Modulation of ROS by TIGAR Correlates with Autophagic Response in Oocytes—ROS functions in the regulation of many cellular responses, including autophagy-an adaptive response to stress conditions such as nutrient starvation and

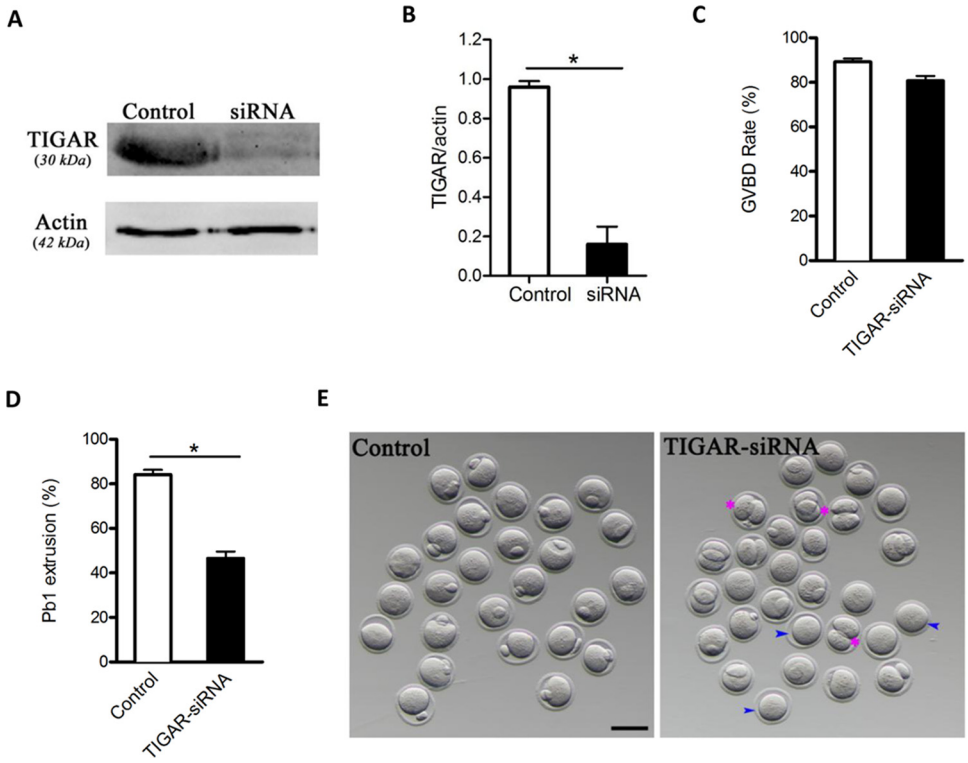

FIG. 3. **Effects of TIGAR knockdown on maturational progression of mouse oocytes.** Fully-grown oocytes microinjected with TIGAR-siRNA were cultured *in vitro* to evaluate the maturational progression. A Negative control siRNA was injected as control. *A*, Knockdown of endogenous TIGAR protein expression after TIGAR-siRNA injection was verified by Western blot analysis (100 oocytes were used for each group). *B*, The ratio of TIGAR/Actin intensity from Western blotting shown in A. Band intensity was calculated using ImageJ software, with actin as a loading control. All experiments were repeated three times and representative images shown. Quantitative analysis of GVBD rate (*C*) and Pb1 extrusion rate (*D*) in control ($n = 120$) and TIGAR-KD ($n = 122$) oocytes. *E*, Phase-contrast images of control and TIGAR-siRNA injected oocytes. Pink asterisks indicate the oocytes with apparent symmetrical division; blue arrowheads indicate the oocytes that fail to extrude polar bodies. Data were expressed as mean ± S.D. from three independent experiments. *$p < 0.05$. Scale bar, 80 μm.

metabolic stress (39, 40). Therefore, we sought to check whether changes in TIGAR expression and the consequent modulation of ROS levels can affect autophagy in mouse oocytes. Autophagy was monitored by evaluating the formation of autophagosomes, as measured in cells by the accumulation of LC3 puncta by fluorescence microscopy. As expected, TIGAR knockdown led to a strong activation of autophagy in either control or HFD oocytes (Fig. 5*A*a,b,c,d-5*B*), whereas TIGAR overexpression significantly reduced the LC3 accumulation in HFD oocytes (Fig. 5*A*c, e-5*B*). Immunoblotting also verified the elevated expression of LC3 protein in HFD oocytes and TIGAR-depleted oocytes relative to controls (Fig. 5*C*). The results indicate a very close correlation between autophagic response and ROS elevation.

To further determine whether the autophagy induced in TIGAR-depleted oocytes was dependent on the elevated ROS, we modulated ROS levels directly by treatment with N-acetyl-L-cystein (NAC), a direct scavenger of ROS. As shown in Fig. 5*D*–5*E*, excessive ROS generation induced by TIGAR knockdown was lowered by the anti-oxidant treatment. NAC also could significantly reduce the ROS levels in HFD oocytes with TIGAR knockdown (supplemental Fig. S1). Correspondingly, the autophagic response was almost completely prevented by ROS scavenger (Fig. 5*F*–5*G*), indicating that the changes in ROS levels seen after TIGAR depletion may be responsible for the effects on autophagy. Altogether, these observations support a notion that modulation of ROS by TIGAR closely associates with autophagic response during mouse oocyte maturation.

Proper Spindle Assembly and Chromosome Alignment in Oocytes Requires TIGAR—The specific positioning of TIGAR to the spindle region prompted us to ask whether TIGAR functions in the assembly of meiotic apparatus in oocytes. For this purpose, control and TIGAR-siRNA injected oocytes were immunolabeled with anti-tubulin antibody to visualize the spindle and counterstained with propidium iodide for chromosomes. Confocal microscopy revealed that most control oocytes at metaphase stage showed a typical barrel-shaped spindle and well-aligned chromosomes at the equatorial plate (Fig. 6*A*a). In sharp contrast, a high frequency of spindle defects and chromosome misalignment was detected when TIGAR was depleted in oocytes (24.9 ± 2.0 *versus* 7.5 ± 1.8% control, $p < 0.05$; Fig. 6Ab,c,d–6*B*), including multipolar spindles, malformed spindles, and scattered chromosomes.

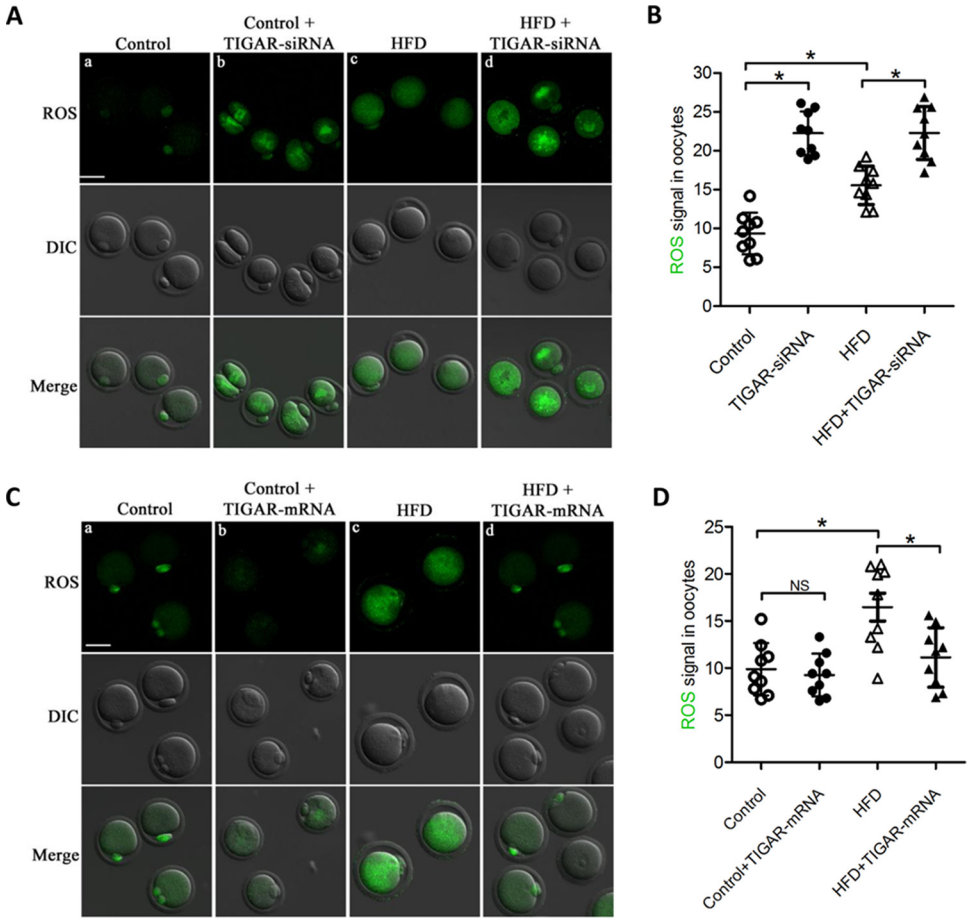

FIG. 4. **TIGAR is involved in ROS accumulation during mouse oocyte maturation.** *A*, Representative images of CM-H_2DCFDA fluorescence in Control, Control+TIGAR-siRNA, HFD, and HFD+TIGAR-siRNA oocytes. *B*, Quantitative analysis of fluorescence intensity shown in *A* ($n = 10$ oocytes for each group). *C,* Representative images of CM-H_2DCFDA fluorescence in Control, Control+TIGAR-mRNA, HFD, and HFD+TIGAR-mRNA oocytes. *D*, Quantitative analysis of fluorescence intensity shown in *C* ($n = 10$ oocytes for each group). All experiments were repeated three times and data were expressed as mean ± S.D. *$p < 0.05$. Scale bar: 50 μm.

These data suggest that the proper assembly of meiotic apparatus in oocytes requires TIGAR.

TIGAR Overexpression Ameliorates Meiotic Defects in Oocytes from HFD Mice—Spindle/chromosome disorganization was readily observed in HFD oocytes (6), which is thought to be associated with excessive ROS. Considering the role of TIGAR during oocyte meiosis, we wished to determine whether elevating the TIGAR expression in HFD oocytes could suppress those defective meiotic phenotypes. To do this, TIGAR mRNA was microinjected into fully-grown HFD oocytes, and then matured oocytes were stained for examining the meiotic apparatus. As shown in Fig. 7, 89.4 ± 1.5% of control oocytes exhibited normal spindle formation and chromosome alignment (with only 10.6% abnormal); however 32.9 ± 2.8% of HFD oocytes showed spindle defects or misaligned chromosomes. Importantly, these anomalies were significantly decreased by ~50% in HFD oocytes overexpressing TIGAR. Collectively, these results suggest that overexpression of TIGAR lowers ROS levels in HFD oocytes and reduces the penetrance of maternal obesity-induced meiotic defects.

DISCUSSION

Obesity is known to be associated with sub-optimal reproductive performance in females. Oxidative stress caused by elevated ROS is a hallmark characteristic of oocytes from obese mice (3). Produced primarily in the mitochondria as a byproduct of respiration, excessive ROS can damage cellular proteins, lipids, and DNA (12, 13). Mammalian oocytes are sensitive to redox imbalance (41), and excessive ROS adversely influences oocyte maturation, fertilization, and subsequent embryo development (42, 43). In this study, by employing knockdown and overexpression experiments, we revealed the function of TIGAR in ROS production in mouse oocytes (Fig. 4). TIGAR has been shown to suppress glycolysis and activate PPP in human cells, leading to the generation of NADPH/GSH and removal of intracellular ROS (16, 44). Notably, oocyte itself has a poor glycolytic activity (21, 25, 45, 46), whereas PPP within the oocytes is important for both nuclear and cytoplasmic maturation as well as cleavage and blastocyst development through the provision of substrates for pu-

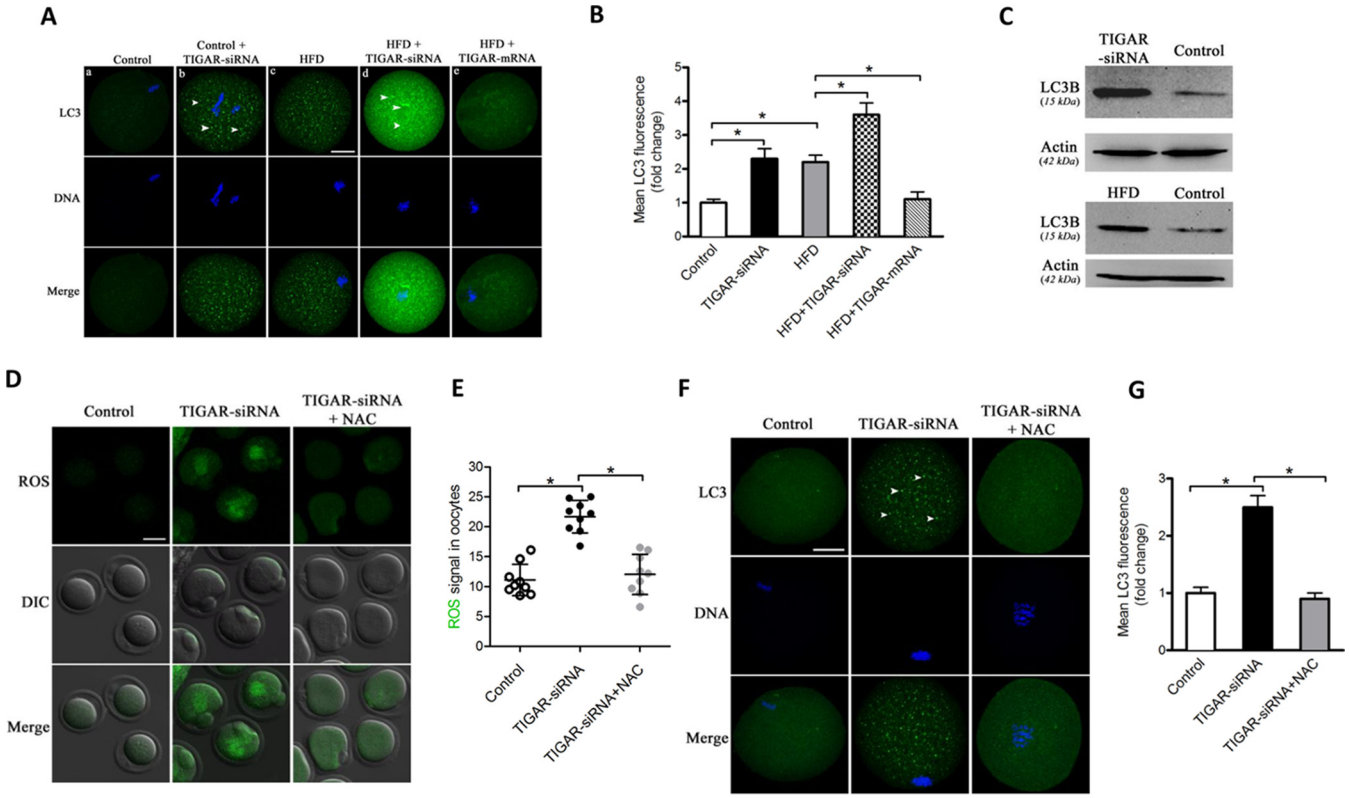

FIG. 5. **TIGAR expression modulates the ROS-dependent autophagy accumulation in oocytes.** *A*, Control, Control+TIGAR-siRNA, HFD, HFD+TIGAR-siRNA, and HFD+TIGAR-mRNA oocytes were labeled with anti-LC3 antibody to visualize the autophagy (green) and counterstained with Hoechst 33342 for chromosomes (blue). Representative confocal sections are shown. Scale bar: 20 μm. *B*, Quantitative analysis of LC3 fluorescence intensity shown in A ($n = 20$ oocytes for each group). *C*, Western blot analysis confirmed the increased LC3B expression in TIGAR-siRNA oocytes and HFD oocytes compared with their controls (250 oocytes for each group). *D*, Representative images of CM-H_2DCFDA fluorescence in Control, Control+TIGAR-siRNA, and TIGAR-siRNA+NAC oocytes. Scale bar: 50 μm. *E*, Quantitative analysis of fluorescence intensity shown in D ($n = 9$ oocytes for each group). *F*, Control, TIGAR-siRNA and TIGAR-siRNA+NAC oocytes were labeled with anti-LC3 antibody to visualize the autophagy (green) and counterstained with Hoechst 33342 for chromosomes (blue). Representative confocal sections are shown. Scale bar: 20 μm. *G*, Quantitative analysis of LC3 fluorescence intensity shown in *F* ($n = 20$ oocytes for each group). All experiments were repeated three times and data were expressed as mean ± S.D. $^*p < 0.05$.

FIG. 6. **TIGAR knockdown disrupt spindle assembly and chromosome organization.** *A*, Control and TIGAR-siRNA-injected oocytes were stained with anti-tubulin antibody to visualize spindle (green) and counterstained with propidium iodide to visualize chromosomes (red). Representative confocal sections are shown. Normal oocytes (a) present a bipolar barrel-shaped spindle and well-aligned chromosomes on the metaphase equator. Spindle defects (arrows) and chromosomes misalignment (arrowheads) were frequently observed in TIGAR-siRNA injected oocytes (b-d). *B*, Quantification of Control and TIGAR-siRNA oocytes with abnormal spindle/chromosomes. Data were expressed as mean ± S.D. from three independent experiments in which at least 120 oocytes were analyzed. $^*p < 0.05$. Scale bar: 20 μm.

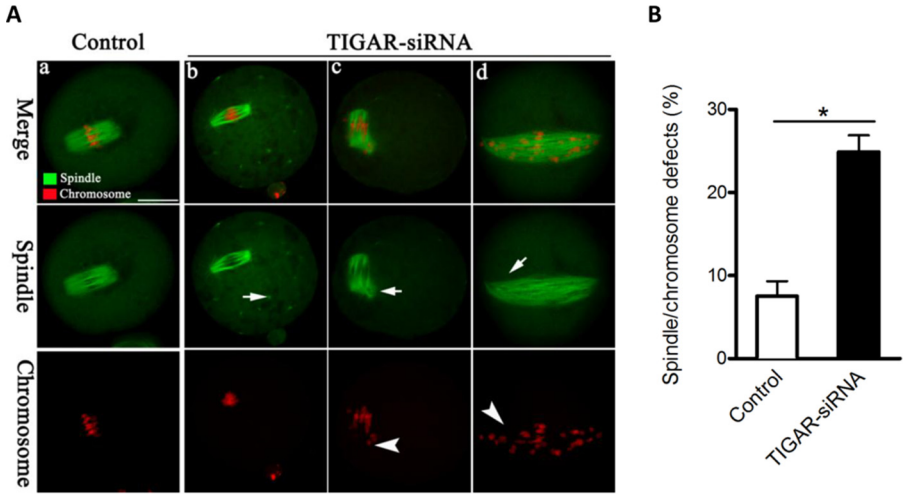

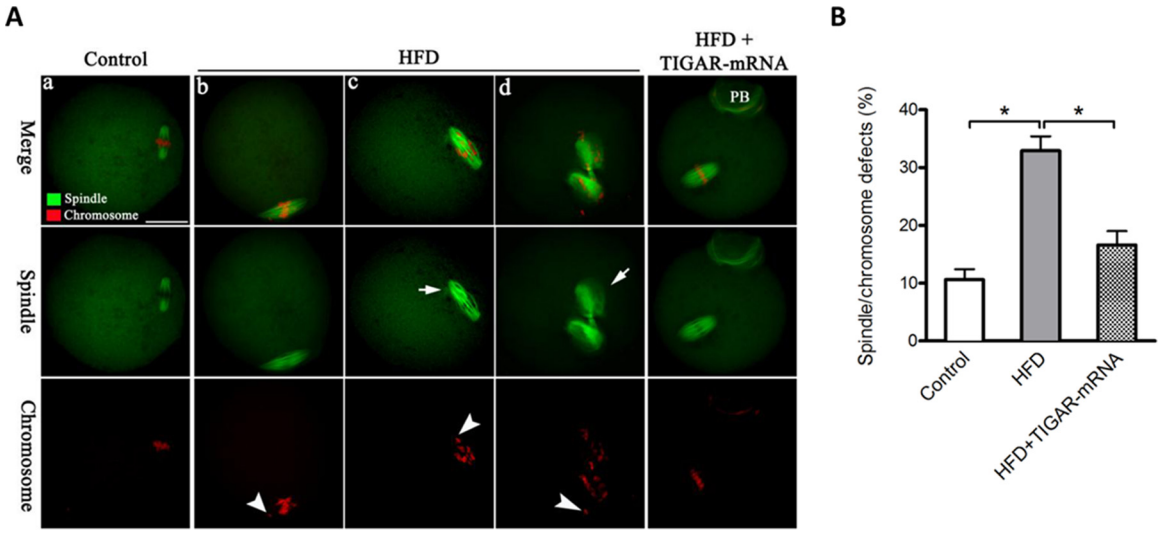

FIG. 7. **TIGAR overexpression alleviates meiotic defects in oocytes from HFD mice.** *A*, Control, HFD and HFD+TIGAR-mRNA oocytes were stained with anti-tubulin antibody to visualize the spindle (green) and counterstained with propidium iodide to visualize chromosomes (red). Representative confocal sections are shown. *B*, Quantification of Control, HFD and HFD+TIGAR-mRNA oocytes with spindle/chromosome defects in *A*. Data were expressed as mean ± S.D. from three independent experiments in which at least 120 oocytes were analyzed. $^*p < 0.05$. Scale bar: 20 μm.

rine synthesis and intra-oocyte redox state (21, 22). Importantly, our proteomic analysis demonstrated that TIGAR protein level was dramatically reduced in HFD oocytes, and ectopic expression of TIGAR was able to ameliorate the oxidative stress in HFD oocytes (Fig. 2 and 4). These data suggest that, on one hand, TIGAR participates in ROS clearance during normal oocyte development; on the other hand, loss of TIGAR is, at least in part, responsible for the ROS stress in oocytes exposed to obese environment. However, the underlying mechanisms mediating this process remain to be investigated. In addition, we found that TIGAR knockdown in oocytes induces autophagy activation dependent on the elevated ROS signals (Fig. 5). Similarly, HFD oocytes with reduced TIGAR expression also showed strong LC3 accumulation (Fig. 5). Autophagy, a mechanism that results in lysosomal degradation of cytoplasmic constituents, is essential for oocyte maturation and embryonic development (47–49). ROS has been identified as signaling molecules in various pathways regulating both cell survival and cell death. In specific, ROS can activate autophagy through several distinct mechanisms involving Atg4, catalase, and the mitochondrial electron transport chain (50, 51). We therefore speculate that the induction of autophagy in response to loss of TIGAR functions a protective response to restrain ROS levels. These results do not, however, preclude the existence of other mechanisms that control autophagy activation in response to maternal obesity. Besides, based on proteomic data, we recently also identified a marked reduction of Stella protein in oocytes from HFD mice (35). Stella is a maternal factor and essential for the global epigenetic remodeling process that occurs soon after fertilization (52, 53). We demonstrate that Stella insufficiency in oocytes contributes to the maternal obesity-associated epigenetic alterations and developmental defects in embryos. Altogether, these findings indicate that the differentially expressed proteins we discovered in this study may mediate the differential effects of obesity on oocyte quality.

Accumulating evidence suggests that oxidative stress is associated with the meiotic defects in oocytes (54). For example, hydroxyl radical generated by the H_2O_2-driven Fenton reaction adversely affects spindle formation and chromosome alignment in mouse oocyte (55). Recently, oxidative stress during meiotic prophase was shown to induce premature loss of cohesion and chromosome segregation errors in oocytes (56). In support of this conception, we simultaneously detected the deficient meiotic apparatus and excessive ROS generation in HFD oocytes (6, 38). Here we revealed that TIGAR depletion in oocytes resulted in the spindle defects and chromosome misalignment (Fig. 6). Strikingly, TIGAR overexpression could partly prevent the maternal obesity-induced meiotic defects in oocytes following the reduction of ROS levels (Fig. 7). These data indicate that the role of TIGAR in the assembly of meiotic structure may be associated with the control of redox state. Intriguingly, we also observed the enrichment of TIGAR protein on the spindle region during oocyte maturation (Fig. 2). Combined with the disrupted meiotic progression in TIGAR-depleted oocytes, we conclude that TIGAR is an essential regulator of oocyte meiosis, which deserves further study.

In summary, well-balanced redox state and accurate control of spindle assembly and chromosome dynamics are the critical determinants for oocyte competence. This study not only uncovers the roles of TIGAR in these processes, but also identifies TIGAR as a target that mediates the effects of maternal obesity on oocyte quality.

DATA AVAILABILITY

The mass spectrometry proteomics data have been deposited to the ProteomeXchange Consortium (http://www.proteomexchange.org) via the PRIDE (57). Project name: Quantitative proteomic analysis of oocytes from high-fat diet (HFD)-fed and normal diet mice; Project accession.

* This work was supported by National Natural Science Foundation of China (NO. 31571543 to QW), National Key R&D Program (2017YFC1001500 to QW; 2016YFA0503300 to XG), and "333 High-level Talent Training Program" of Jiangsu Province (BRA2016386 to XG).

S This article contains supplemental material.

** To whom correspondence should be addressed: State Key Laboratory of Reproductive Medicine, Nanjing Medical University, 101 Longmian Rd, Nanjing, Jiangsu, 211166 China. Tel. and Fax: +86-25-86869511; E-mail: qwang2012@njmu.edu.cn or Tel. and Fax: +86-25-86869383; E-mail: guo_xuejiang@njmu.edu.cn.

‡‡ These authors contributed equally to this work.

Author contributions: H.W., X.G., and Q.W. designed research; H.W., Q.C., X.L., L.H., L.L., H.Z., Y.G., G.W., and J.G. performed research; H.W., X.G., and Q.W. analyzed data; H.W., X.G., and Q.W. wrote paper.

REFERENCES

1. Metwally, M., Li, T. C., and Ledger, W. L. (2007) The impact of obesity on female reproductive function. *Obesity Rev.* **8,** 515–523
2. Jungheim, E. S., and Moley, K. H. (2010) Current knowledge of obesity's effects in the pre- and periconceptional periods and avenues for future research. *Am. J. Obstetrics Gynecol.* **203,** 525–530
3. Natalia Igosheva, A. Y. A., Lucilla Poston Judith J., Eckert, Tom P., Fleming, Michael, R., and Duchen, J. M. (2010) Maternal diet-induced obesity alters mitochondrial activity and redox status in mouse oocytes and zygotes. *PLoS ONE* **5,** e10074
4. Dionne C Gesink Law, R. F. M, and Matthew P Longnecker. (2007) Obesity and time to pregnancy. *Hum. Reprod.* **22,** 414–420
5. Grindler, N. M., and Moley, K. H. (2013) Maternal obesity, infertility and mitochondrial dysfunction: potential mechanisms emerging from mouse model systems. *Mol. Human Reproduction* **19,** 486–494
6. Luzzo, K. M., Wang, Q., Purcell, S. H., Chi, M., Jimenez, P. T., Grindler, N., Schedl, T., and Moley, K. H. (2012) High fat diet induced developmental defects in the mouse: oocyte meiotic aneuploidy and fetal growth retardation/brain defects. *PLoS ONE* **7,** e49217
7. Robker, R. L. (2008) Evidence that obesity alters the quality of oocytes and embryos. *Pathophysiology* **15,** 115–121
8. Linné, Y. (2004) Effects of obesity on women's reproduction and complications during pregnancy. *Obesity Rev.* **5,** 137–143
9. Deleted in proof
10. Luke, B., Brown, M. B., Missmer, S. A., Bukulmez, O., Leach, R., Stern, J. E., and Society for Assisted Reproductive Technology writing, g. (2011) The effect of increasing obesity on the response to and outcome of assisted reproductive technology: a national study. *Fertility Sterility* **96,** 820–825
11. Hou, Y. J., Zhu, C. C., Duan, X., Liu, H. L., Wang, Q., and Sun, S. C. (2016) Both diet and gene mutation induced obesity affect oocyte quality in mice. *Sci. Reports* **6,** 18858
12. Brookes, P. S., Ll, A., Shiva. S., Sarti, P., and Mdarley-Usmar, V. (2002) Mitochondria: regulators of signal transduction by reactive oxygen and nitrogen species. *Free Radical Biol. Med.* **33,** 755–764
13. Balaban, R. S., Nemoto, S., and Finkel, T. (2005) Mitochondria, oxidants, and aging. *Cell* **120,** 483–495
14. Yin, L., Kosugi, M., and Kufe, D. (2012) Inhibition of the MUC1-C oncoprotein induces multiple myeloma cell death by down-regulating TIGAR expression and depleting NADPH. *Blood* **119,** 810–816
15. Cheung, E. C., Lee, P., Ceteci, F., Nixon, C., Blyth, K., Sansom, O. J., and Vousden, K. H. (2016) Opposing effects of TIGAR- and RAC1-derived ROS on Wnt-driven proliferation in the mouse intestine. *Genes Develop.* **30,** 52–63
16. Bensaad, K., Tsuruta, A., Selak, M. A., Vidal, M. N., Nakano, K., Bartrons, R., Gottlieb, E., and Vousden, K. H. (2006) TIGAR, a p53-inducible regulator of glycolysis and apoptosis. *Cell* **126,** 107–120
17. Li, H., and Jogl, G. (2009) Structural and biochemical studies of TIGAR (TP53-induced glycolysis and apoptosis regulator). *J. Biol. Chem.* **284,** 1748–1754
18. Lee, P., Vousden, K. H., Cheung, E. C. (2014) TIGAR, TIGAR, burning bright. *Cancer Metabolism* **2**
19. Wanka, C., Steinbach, J. P., and Rieger, J. (2012) Tp53-induced glycolysis and apoptosis regulator (TIGAR) protects glioma cells from starvation-induced cell death by up-regulating respiration and improving cellular redox homeostasis. *J. Biol. Chem.* **287,** 33436–33446
20. Xie, J. M., Li, B., Yu, H. P., Gao, Q. G., Li, W., Wu, H. R., and Qin, Z. H. (2014) TIGAR has a dual role in cancer cell survival through regulating apoptosis and autophagy. *Cancer Res.* **74,** 5127–5138
21. Sutton-McDowall, M. L., Gilchrist, R. B., and Thompson, J. G. (2010) The pivotal role of glucose metabolism in determining oocyte developmental competence. *Reproduction* **139,** 685–695
22. Herrick, J. R., Brad, A. M., and Krisher, R. L. (2006) Chemical manipulation of glucose metabolism in porcine oocytes: effects on nuclear and cytoplasmic maturation in vitro. *Reproduction* **131,** 289–298
23. Xie, H. L., Wang, Y. B., Jiao, G. Z., Kong, D. L., Li, Q., Li, H., Zheng, L. L., and Tan, J. H. (2016) Effects of glucose metabolism during in vitro maturation on cytoplasmic maturation of mouse oocytes. *Sci. Reports* **6,** 20764
24. Alvarez, G. M., Casiro, S., Gutnisky, C., Dalvit, G. C., Sutton-McDowall, M. L., Thompson, J. G., and Cetica, P. D. (2016) Implications of glycolytic and pentose phosphate pathways on the oxidative status and active mitochondria of the porcine oocyte during IVM. *Theriogenology* **86,** 2096–2106
25. Gu, L., Liu, H., Gu, X., Boots, C., Moley, K. H., and Wang, Q. (2015) Metabolic control of oocyte development: linking maternal nutrition and reproductive outcomes. *Cell. Mol. Life Sci.* **72,** 251–271
26. Qi, L., Liu, Z., Wang, J., Cui, Y., Guo, Y., Zhou, T., Zhou, Z., Guo, X., Xue, Y., and Sha, J. (2014) Systematic analysis of the phosphoproteome and kinase-substrate networks in the mouse testis. *Mol. Cell. Proteomics* **13,** 3626–3638
27. Wang, J., Qi, L., Huang, S., Zhou, T., Guo, Y., Wang, G., Guo, X., Zhou, Z., and Sha, J. (2015) Quantitative phosphoproteomics analysis reveals a key role of insulin growth factor 1 receptor (IGF1R) tyrosine kinase in human sperm capacitation. *Mol. Cell. Proteomics* **14,** 1104–1112
28. Cox, J., and Mann, M. (2008) MaxQuant enables high peptide identification rates, individualized p.p.b.-range mass accuracies and proteome-wide protein quantification. *Nature Biotechnol.* **26,** 1367–1372
29. Magrane, M., and UniProt, C. (2011) UniProt Knowledgebase: a hub of integrated protein data. *Database* 2011, bar009
30. Schwanhausser, B., Busse, D., Li, N., Dittmar, G., Schuchhardt, J., Wolf, J., Chen, W., and Selbach, M. (2011) Global quantification of mammalian gene expression control. *Nature* **473,** 337–342
31. de Hoon, M. J., Imoto, S., Nolan, J., and Miyano, S. (2004) Open source clustering software. *Bioinformatics* **20,** 1453–1454
32. Huang da, W, Sherman, B. T., and Lempicki, R. A. (2009) Systematic and integrative analysis of large gene lists using DAVID bioinformatics resources. *Nature Protocols* **4,** 44–57
33. Wang, Q., Chi, M. M., and Moley, K. H. (2012) Live imaging reveals the link between decreased glucose uptake in ovarian cumulus cells and impaired oocyte quality in female diabetic mice. *Endocrinology* **153,** 1984–1989
34. Cho, W. C. (2007) Proteomics technologies and challenges. *Genomics Proteomics Bioinformatics* **5,** 77–85
35. Han, L., Ren, C., Li, L., Li, X., Ge, J., Wang, H., Miao, Y. L., Guo, X., Moley, K. H., Shu, W., and Wang, Q. (2018) Embryonic defects induced by maternal obesity in mice derive from Stella insufficiency in oocytes. *Nat. Genet.* **50,** 432–442
36. Li, M., Sun, M., Cao, L., Gu, J. H., Ge, J., Chen, J., Han, R., Qin, Y. Y., Zhou, Z. P., Ding, Y., and Qin, Z. H. (2014) A TIGAR-regulated metabolic pathway is critical for protection of brain ischemia. *J. Neurosci.* **34,** 7458–7471
37. Ye, L., Zhao, X., Lu, J., Qian, G., Zheng, J. C., and Ge, S. (2013) Knockdown of TIGAR by RNA interference induces apoptosis and autophagy in

HepG2 hepatocellular carcinoma cells. *Biochem. Biophys. Res. Commun.* **437,** 300–306
38. Zhang, L., Han, L., Ma, R., Hou, X., Yu, Y., Sun, S., Xu, Y., Schedl, T., Moley, K. H., and Wang, Q. (2015) Sirt3 prevents maternal obesity-associated oxidative stress and meiotic defects in mouse oocytes. *Cell Cycle* **14,** 2959–2968
39. Mizushima, N. (2007) Autophagy: process and function. *Genes Development* **21,** 2861–2873
40. Bang, S., Shin, H., Song, H., Suh, C. S., and Lim, H. J. (2014) Autophagic activation in vitrified-warmed mouse oocytes. *Reproduction* **148,** 11–19
41. Lin Liu James Trimarchi, R., and Keefe a, DL. (2000) Involvement of mitochondria in oxidative stress-induced cell death in mouse zygotes. *Biol. Reprod.* **62,** 1745–1753
42. Alexandra J., Harvey, J., KLKa, G. T. (2002) REDOX regulation of early embryo development. *Reproduction* **123,** 479–486
43. Bedaiwy, M. A., Falcone, T., Mohamed, M. S., Aleem, A. A., Sharma, R. K., Worley, S. E., Thornton, J., and Agarwal, A. (2004) Differential growth of human embryos in vitro: role of reactive oxygen species. *Fertility Sterility* **82,** 593–600
44. Green, D. R., and Chipuk, J. E. (2006) p53 and metabolism: Inside the TIGAR. *Cell* **126,** 30–32
45. Biggers, JD.W. D, Donahue, . R. P.. (1967) The pattern of energy metabolism in the mouse oocyte and zygote. *Proc. Natl. Acad. Sci. U.S.A.* **58,** 560–567
46. Harris, S. E., Adriaens, I., Leese, H. J., Gosden, R. G., and Picton, H. M. (2007) Carbohydrate metabolism by murine ovarian follicles and oocytes grown in vitro. *Reproduction* **134,** 415–424
47. Song, B. S., Kim, J. S., Kim, Y. H., Sim, B. W., Yoon, S. B., Cha, J. J., Choi, S. A., Yang, H. J., Mun, S. E., Park, Y. H., Jeong, K. J., Huh, J. W., Lee, S. R., Kim, S. H., Kim, S. U., and Chang, K. T. (2014) Induction of autophagy during in vitro maturation improves the nuclear and cytoplasmic maturation of porcine oocytes. *Reproduction, Fertility, Development* **26,** 974–981
48. Satoshi Tsukamoto, A. K. N. M.. (2008) The role of autophagy during the oocyte-to-embryo transition. *Autophagy* **4,** 1076–1078
49. Adastra, K. L., Chi, M. M., Riley, J. K., and Moley, K. H. (2011) A differential autophagic response to hyperglycemia in the developing murine embryo. *Reproduction* **141,** 607–615
50. Bensaad, K., Cheung, E. C., and Vousden, K. H. (2009) Modulation of intracellular ROS levels by TIGAR controls autophagy. *EMBO J.* **28,** 3015–3026
51. Yongqiang Chen, E. M.-W., Jiming Kong Sara Israels, J., and Spencer BGibson . (2007) Mitochondrial electron-transport-chain inhibitors of complexes I and II induce autophagic cell death mediated by reactive oxygen species. *J. Cell Sci.* **120**, 4155–4166
52. Nakamura, T., Liu, Y. J., Nakashima, H., Umehara, H., Inoue, K., Matoba, S., Tachibana, M., Ogura, A., Shinkai, Y., and Nakano, T. (2012) PGC7 binds histone H3K9me2 to protect against conversion of 5mC to 5hmC in early embryos. *Nature* **486,** 415–419
53. Wossidlo, M., Nakamura, T., Lepikhov, K., Marques, C. J., Zakhartchenko, V., Boiani, M., Arand, J., Nakano, T., Reik, W., and Walter, J. (2011) 5-Hydroxymethylcytosine in the mammalian zygote is linked with epigenetic reprogramming. *Nat. Commun.* **2,** 241
54. Zhang, X., Wu, X. Q., Lu, S., Guo, Y. L., and Ma, X. (2006) Deficit of mitochondria-derived ATP during oxidative stress impairs mouse MII oocyte spindles. *Cell Res.* **16,** 841–850
55. Shaeib, F., Banerjee, J., Maitra, D., Diamond, M. P., and Abu-Soud, H. M. (2013) Impact of hydrogen peroxide-driven Fenton reaction on mouse oocyte quality. *Free Radic. Biol. Med.* **58,** 154–159
56. Perkins, A. T., Das, T. M., Panzera, L. C., and Bickel, S. E. (2016) Oxidative stress in oocytes during midprophase induces premature loss of cohesion and chromosome segregation errors. *Proc. Natl. Acad. Sci. U.S.A.* **113,** E6823–E6830
57. Vizcaino, J. A., Deutsch, E. W., Wang, R., Csordas, A., Reisinger, F., Rios, D., Dianes, J. A., Sun, Z., Farrah, T., Bandeira, N., Binz, P. A., Xenarios, I., Eisenacher, M., Mayer, G., Gatto, L., Campos, A., Chalkley, R. J., Kraus, H. J., Albar, J. P., Martinez-Bartolome, S., Apweiler, R., Omenn, G. S., Martens, L., Jones, A. R., and Hermjakob, H. (2014) ProteomeXchange provides globally coordinated proteomics data submission and dissemination. *Nat. Biotechnol.* **32,** 223–226